Audio Engineering Society

Conference Paper 17

Presented at the AES International Conference on Headphone Technology
2025 August 27-29, Espoo, Finland

This conference paper was selected based on a submitted abstract and 750-word precis that have been peer reviewed by at least two qualified anonymous reviewers. The complete manuscript was not peer reviewed. This conference paper has been reproduced from the author's advance manuscript without editing, corrections, or consideration by the Review Board. The AES takes no responsibility for the contents. This paper is available in the AES E-Library (http://www.aes.org/e-lib), all rights reserved. Reproduction of this paper, or any portion thereof, is not permitted without direct permission from the Journal of the Audio Engineering Society.

Estimating the Sound Pressure at the Eardrum and Ear Canal Transfer Function with In-Ear Headphones

Etienne Rivet[1], Calum Smeaton[1], Jeong-Woo Kim[1], Todd Welti[1], Sean Olive[1], and Jeff Baker[1]

[1]Harman International Industries, Northridge, CA, USA

Correspondence should be addressed to Etienne Rivet (etienne.rivet@harman.com)

ABSTRACT

When inserting an in-ear headphone (or earphone) in users' ears, it is loaded by a range of ear canal geometries and eardrum impedances which interact with the output impedance of the sound source. As a result, the ear canal transfer function between the ear tip and eardrum exhibits ear canal resonances above 1 kHz that may vary by one octave for the first resonance and around 10 dB between ears. The target responses for music reproduction and hear-through, which were originally tuned in an ear simulator, are thus altered at the users' ears. We propose a new approach without making assumptions about ear canal geometry or eardrum impedance. The relationship between voltage, pressure and volume velocity of the earphone, which includes an in-ear microphone, are first characterized to turn the device into a pressure-volume velocity sensor. Then, the response of the in-ear microphone which is affected by the acoustic loading of the individual ear is used to calculate the input impedance of the ear. This ear impedance is then used to reconstruct the ear canal transfer function from the ear tip up to the user's eardrum. Finally, the response at the user's eardrum can be estimated knowing the pressure at the ear tip and this ear canal transfer function. Results in Type 2 and Type 4.3 artificial ears showed a high accuracy up to 9 kHz. They are compared to other estimations in human ears.

1 Introduction

The frequency responses of earphones are usually tuned in artificial ears to provide a desired target curve at the drum reference point (DRP), which corresponds to the preferred sound quality based on listening tests [1]. Also, hear-through (HT) and active noise cancellation (ANC) modes are pre-calibrated – even though updated in-situ in users' ears - to reproduce naturally the external sounds and attenuate the noise. Because of limitations for the Type 3.3 artificial ears for earphones [2], the Type 4.3 simulator was designed with an anatomical ear canal simulator to represent an average human ear based on ear impedance measurements [3]. However, there is a high variability of the ear anatomy with different ear canal geometries [4, 5] and eardrum impedance values [6]. For example, the first ear canal resonance frequency varies by one octave and 10 dB among individuals' ears. When the earphone is inserted in users' ears, the output impedance of the audio device is coupled to the input impedance of the ear at the ear tip [7], modifying significantly the shapes of the ear canal resonances, both in frequency and magnitude. As a result, sound is not reproduced as expected at users' eardrums and ANC performance may decrease. These observations justify the need for individualized compensation, which requires the prediction of the sound pressure at the eardrum for sound reproduction and ear canal transfer function for ANC / HT applications.

Probe microphones are often used to measure the sound pressure at the eardrum. However, this method is not only invasive and difficult to set up, but it also shows its limitations as the measured sound pressure deviates at high frequencies with even small distances from the eardrum [8]. An alternative is the pressure-minima method, which estimates the first one or two resonances based on local minima of pressure for tube- and cone-based ear canal models [9, 10]. As the pressure-minima method may not work depending on the source impedance or microphone location, the reflectance of the measured impedance at the ear canal entrance was proposed. The reflectance phase was then used as a cost optimization function to estimate the ear canal geometry via the area function [11, 12], or the pressure at the eardrum via ear canals modeled through a tube, cone, or portions of short tubes [9, 13, 14]. Alternatively, the absorbed power or energy, and forward pressure techniques were also proposed by using a probe [15] or directly using a pressure-velocity sensor [16]. Linear regression models were also found between the earphone and ear [17]. Most of these methods, which assumed the eardrum impedance as highly resistive or used models among the ones reviewed in [18], may constrain the predicted values for the pressure at DRP and transfer functions. The proposed approach is to estimate the pressure at DRP without making assumptions on the ear canal geometry and eardrum impedance.

In Section 2, we show that the pressure can be expressed as a modal expansion of the ear canal resonances based on the wave equation. We present the calibration method to turn any earphone into a pressure-volume velocity sensor in Section 3. The measurement of the ear impedance and pressure at the ear tip is introduced in Section 4. Then, we show how to estimate the modal parameters of the ear canal resonances from this measured impedance in Section 5. Finally, the method is evaluated in Type 2 and Type 4.3 artificial ears in Section 6. The results are compared to other estimations in human ears in Section 7 and followed by a discussion in Section 8.

2 Modal Expansion of the Ear Canal Transfer Function

Even though ear canals are 3-dimensional geometries, we consider only one axis. It has been shown that the effect of curvature modifies the resonance frequencies, and that these may be modeled by length corrections [19]. As we are interested in the transfer function of pressures between the earphone output and the eardrum, we write the Webster's or horn wave equation via the volume velocity $U(x,\omega)$ (or flow rate) with a source pressure at the input in the frequency domain using the Fourier transform along the x axis as

$$\frac{\partial^2 \mathrm{U}}{\partial \mathrm{x}^2} - \frac{Y_t'}{Y_t}\frac{\partial \mathrm{U}}{\partial \mathrm{x}} - \Gamma^2 U = -Y_{t0} P_s \delta(x) \tag{1}$$

where ω is the angular frequency, $\Gamma = \sqrt{Z_v Y_t}$ is the propagation constant ($\Gamma = jk$ where j is the imaginary unit and k is the complex wavenumber), $Z_v(x)$ and $Y_t(x)$ are the viscous and thermal conduction effects that depend on the cross-section area $S(x)$, and $P_s(0,\omega)$ is the sound pressure applied at the source located at $x = 0$ [20]. We assume that the eardrum is located at DRP at $x = L$ and perpendicular to the x axis, which is further discussed in Section 8. We also assume that the real part of the eardrum impedance $Z_{DRP}(\omega)$ is higher than the characteristic impedance $Z_c = \sqrt{Z_v/Y_t}$ at $x = L$, i.e. $\Re(Z_{DRP}(\omega)) > Z_{cL}$.

Our proposed approach is the modal decomposition of the solution of the wave equation via Green's function in the frequency domain. Therefore we seek solutions to Eq. (1) of the form $U(x,\omega) = \sum_n A_n(\omega)\phi_n(x)$, where the amplitudes $A_n(\omega)$ are associated with the modes $\phi_n(x)\exp(j\omega t)$. Expressing the pressure $P_s(0,\omega)$ at the source and assuming a high eardrum impedance $Z_{DRP}(\omega)$ results in a Dirichlet boundary condition at $x = 0$ and approximately a Neumann boundary condition at $x = L$, which is close to an open-closed tube configuration. For these boundary conditions, the modes are orthogonal for

$$\int_0^L S^{-1}(x)\phi_m(x)\phi_n(x) = \Lambda_{mn}\delta_{mn} \tag{2}$$

We write the modal expansion of the input ear impedance as follows

$$Z_{EC}(\omega) = \frac{Z_{c0}}{j\omega}\frac{1}{\sum_{n>0}\frac{F_n}{{\omega_{0,n}}^2 - \omega^2 + 2j\omega\zeta_{0,n}\omega_{0,n}}} \tag{3}$$

where F_n is a coefficient depending on the eigenmodes ϕ_n, $\omega_{0,n}$ is the natural angular frequency, $\zeta_{0,n}$ is the damping coefficient associated to the mode n [20]. The eigenfrequencies can be calculated as $\omega_n = \omega_{0,n}\sqrt{1 - {\zeta_{0,n}}^2}$.

The solution of Eq. (1), which corresponds to the transfer admittance, is written after deriving the Green's function as

$$U(x,\omega) = Y_{t0}P_s c^2 \sum_{n>1} \frac{\phi_n(x)\phi_n(0)}{\Lambda_n\left({\omega_{0,n}}^2 - \omega^2 + 2j\omega\zeta_{0,n}\omega_{0,n}\right)} \quad (4)$$

which is valid for $x \neq 0$ [20]. The modal expansion of the pressure can then be calculated as

$$P(x,\omega) = -P_s c^2 \sum_{n>1} \frac{\phi_n(0)\,\partial\phi_n(x)/\,\partial \mathrm{x}}{\Lambda_n\left({\omega_{0,n}}^2 - \omega^2 + 2j\omega\zeta_{0,n}\omega_{0,n}\right)} \quad (5)$$

where c is the speed of sound in air. Obviously, eigenmodes $\phi_n(x)$ cannot be calculated without knowing the ear canal geometry. However, we are interested in identifying the pressure $P(L,\omega)$ at DRP in function of the source $P_s(\omega)$ and not at intermediate positions. We start with the cylindrical tube ansatz that the eigenmodes are $\phi_n(x) = \cosh(\Gamma(\mathrm{s}_n)x)$, where s_n are the poles corresponding to the mode n. We have validated this with simulations of modeled eardrum impedances $Z_{DRP}(\omega)$ as in [18] and ear canals modeled through many small segments of truncated cones, whose total distance from the apex of this equivalent "cone" to the entrance is small compared to the wavelength [11, 12]. As we do not know which parameters of the poles depend on the x axis, we simply choose $\Gamma'(\mathrm{s}_n) = \omega_n/c$ in the derivative term of $\partial\phi_n(x)/\,\partial$x in Eq. (5).

Finally, an approximation of the modal expansion of the ear canal transfer function from the source $P_s(\omega)$ to the estimated pressure $\hat{P}_{DRP}(\omega)$ at DRP by truncating the first N modes is proposed as follows

$$H_{\hat{P}_{DRP}/P_s}(\omega) \approx G_0 \sum_{n=1}^{N} \frac{(-1)^{n-1}\omega_n}{{\omega_{0,n}}^2 - \omega^2 + 2j\omega\zeta_{0,n}\omega_{0,n}} \quad (6)$$

Instead of estimating the term Λ_n, we use the property of a constant pressure field in the ear at low frequencies. We simply choose the gain G_0 such that $\left|H_{\hat{P}_{DRP}/P_s}(\omega)\right|_{\omega\to 0} = 1$.

While Eq. (6) is valid for different ear canal geometries and eardrum impedance values, Eq. (4) does not hold for the transfer admittance $H_{U_{DRP}/P_s}(\omega)$ that is written at $x = L$ for complex termination impedances. It justifies why we chose to express the wave equation via the volume velocity in Eq. (1) with a pressure at the source and not via the pressure with a source volume velocity. The modal parameters in Eq. (6) can be estimated from the ear impedance in Eq. (3). In Section 3, we present the use of earphones as pressure-volume velocity sensor, and in Section 4, we present a technique for getting the impedance $Z_{EC}(\omega)$ and the pressure $P_s(\omega)$. With these quantities, we can ultimately return to Eq. (6) to yield the pressure at DRP in Section 5.

3 Turning the Earphone into a Pressure – Volume Velocity Sensor

To measure the ear impedance $Z_{EC}(\omega)$ at the ear tip, we need to characterize the earphone by turning it into a pressure-volume velocity sensor, on top of its sound source capabilities. Similar methods can be found in [3, 9, 14]. We define the voltage $E_{DRV}(\omega)$ and current $I_{DRV}(\omega)$ at driver terminals of the earphone, the pressure $P_{EP}(\omega)$ and volume velocity $U_{EP}(\omega)$ at the ear tip output, the pressure $P_{MIC}(\omega)$ and volume velocity $U_{MIC}(\omega)$ at the in-ear microphone, as illustrated in Fig. 1. Instead of modeling and identifying every electroacoustic element of the earphone, we represent the system by two two-port networks (TPN) $\boldsymbol{T_{EP}}$ and $\boldsymbol{T_{EP2}}$ with matrix elements $a_{ij}(\omega)$ and $d_{ij}(\omega)$ respectively. We do not use an additional possible TPN $\boldsymbol{T_{EP1}}$, whose inputs are the voltage $E_{DRV}(\omega)$ and current $I_{DRV}(\omega)$ and outputs are the pressure $P_{MIC}(\omega)$ and volume velocity $U_{MIC}(\omega)$.

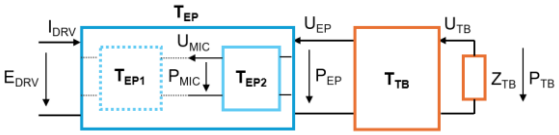


Figure 1. Two-port network representation of the earphone in a calibration tube.

The earphones are inserted in N calibration tubes that are each terminated by a measurement microphone. We define the pressure $P_{TB}(\omega)$ and volume velocity $U_{TB}(\omega)$, and the termination impedance $Z_{TB}(\omega) = -P_{TB}(\omega)/U_{TB}(\omega)$. Each tube n is also represented by a TPN $\boldsymbol{T_{TB,n}}$ with matrix elements $b_{ij}(\omega)$. For cylindrical tubes, the TPN $\mathbf{T}_{\boldsymbol{TB,n}}$ of the tube n is modeled as a transmission line as follows

$$\mathbf{T}_{\boldsymbol{TB,n}} = \begin{pmatrix} \cosh(\Gamma l_n) & Z_c\sinh(\Gamma l_n) \\ \sinh(\Gamma l_n)/Z_c & \cosh(\Gamma l_n) \end{pmatrix} \quad (7)$$

where l_n is the length of the calibration tube n. Here, all the tubes have the same diameter, hence a single value for the characteristic impedance Z_c. Measuring the pressure $P_{TB,n}(\omega)$ in N calibration tubes (at least 2) gives the estimation of the matrix elements

$[a_{11}(\omega), a_{12}(\omega)]$ of $\boldsymbol{T_{EP}}$ using the Moore-Penrose pseudoinverse

$$\begin{pmatrix} a_{11}(\omega) \\ a_{12}(\omega) \end{pmatrix} = (\boldsymbol{T_m}^* \boldsymbol{T_m})^{-1} \boldsymbol{T_m}^* \begin{pmatrix} 1 \\ \overline{H_{P_{TB}/E_{DRV},1}(\omega)} \\ \vdots \\ 1 \\ \overline{H_{P_{TB}/E_{DRV},N}(\omega)} \end{pmatrix} \tag{8}$$

where $H_{P_{TB}/E_{DRV},n}(\omega)$ is the measured pressure response of $P_{TB,n}(\omega)$ with drive voltage $E_{DRV,n}(\omega)$,

$$\boldsymbol{T_m} = \begin{pmatrix} b_{11,1}(\omega) + \dfrac{b_{12,1}(\omega)}{Z_{TB}(\omega)} & b_{21,1}(\omega) + \dfrac{b_{22,1}(\omega)}{Z_{TB}(\omega)} \\ \vdots & \vdots \\ b_{11,\mathrm{N}}(\omega) + \dfrac{b_{12,\mathrm{N}}(\omega)}{Z_{TB}(\omega)} & b_{21,\mathrm{N}}(\omega) + \dfrac{b_{22,\mathrm{N}}(\omega)}{Z_{TB}(\omega)} \end{pmatrix} \tag{9}$$

and $\boldsymbol{T_m}^*$ is its conjugate transpose. Similarly, the matrix elements $[d_{11}(\omega), d_{12}(\omega)]$ of $\boldsymbol{T_{EP2}}$ are estimated as

$$\begin{pmatrix} d_{11}(\omega) \\ d_{12}(\omega) \end{pmatrix} = (\boldsymbol{T_m}^* \boldsymbol{T_m})^{-1} \boldsymbol{T_m}^* \begin{pmatrix} 1 \\ \overline{H_{P_{TB}/P_{MIC},1}(\omega)} \\ \vdots \\ 1 \\ \overline{H_{P_{TB}/P_{MIC},N}(\omega)} \end{pmatrix} \tag{10}$$

where $H_{P_{TB}/P_{MIC},n}(\omega)$ is the measured transfer function of $P_{TB,n}(\omega)$ with pressure $P_{MIC,n}(\omega)$. The calibrated elements $[a_{11}(\omega), a_{12}(\omega)]$ of $\boldsymbol{T_{EP}}$ and $[d_{11}(\omega), d_{12}(\omega)]$ of $\boldsymbol{T_{EP2}}$ are used to determine implicitly the acoustic quantities at the ear tip knowing the voltage $E_{DRV}(\omega)$ and pressure $P_{MIC}(\omega)$. The measurement of the input impedance of users' ears is presented in Section 4.

4 Measuring the User's Ear Impedance

When the earphone is inserted in the user's ear, the ear corresponds to an acoustic load $Z_{EC}(\omega) = -P_{EP}(\omega)/U_{EP}(\omega)$ for the earphone at the ear tip. Each of the TPNs $\boldsymbol{T_{EP}}$ and $\boldsymbol{T_{EP2}}$ has a relationship between $H_{P_{EP}/E_{DRV}}(\omega)$ and $Z_{\mathrm{EC}}(\omega)$ as

$$H_{P_{EP}/E_{DRV}}(\omega) = \frac{1}{a_{11}(\omega) + a_{12}(\omega)/Z_{EC}(\omega)} \tag{11}$$

$$H_{P_{EP}/E_{DRV}}(\omega) = \frac{H_{P_{MIC}/E_{DRV}}(\omega)}{d_{11}(\omega) + d_{12}(\omega)/Z_{EC}(\omega)} \tag{12}$$

The user's ear impedance at the ear tip can then be calculated using Eqs. (11, 12) as

$$Z_{EC}(\omega) = \frac{H_{P_{MIC}/E_{DRV}}(\omega)a_{12}(\omega) - d_{12}(\omega)}{d_{11}(\omega) - H_{P_{MIC}/E_{DRV}}(\omega)a_{11}(\omega)} \tag{13}$$

Similarly, the frequency response $H_{P_{EP}/E_{DRV}}(\omega)$ at the ear tip can be calculated using Eqs. (11, 13) as

$$H_{P_{EP}/E_{DRV}}(\omega) = \frac{H_{P_{MIC}/E_{DRV}}(\omega)a_{12}(\omega) - d_{12}(\omega)}{a_{12}(\omega)d_{11}(\omega) - a_{11}(\omega)d_{12}(\omega)} \tag{14}$$

Thanks to the calibration process of the earphone described in Section 3, the ear impedance $Z_{EC}(\omega)$ and acoustic quantities can be measured at the ear tip. The amount of fit leakage is even captured at low frequencies in the measured pressure response $H_{P_{EP}/E_{DRV}}(\omega)$ and impedance $Z_{EC}(\omega)$, when the ear tip is not sealed in the users' ears. An alternative approach, which is not described in the paper, is to measure the current $I_{DRV}(\omega)$ instead of the pressure $P_{MIC}(\omega)$ of the in-ear microphone.

5 Estimating the Eigenfrequencies and Sound Pressure at the Eardrum

After measuring the user's ear impedance $Z_{EC}(\omega)$, we need to estimate the modal parameters of the first *N* modes as highlighted in Eqs. (3-6). They can be determined from the poles of the measured input admittance $Y_{EC}(\omega)$. We use the rational fractional polynomials method [21], which has low computation requirements and high processing speed. Using orthogonal polynomials, the denominator polynomial coefficients of the admittance $Y_{EC}(\omega)$ are fit by minimizing an error function between the measured function and the analytical model. The number of poles and zeros are specified within the limited frequency range surrounding the resonance peaks. After estimating the modal parameters of the first *N* modes, the ear canal transfer function can be modeled using Eq. (6). Finally, the pressure response at DRP is estimated from Eqs. (6, 14) as follows

$$H_{\hat{P}_{DRP}/E_{DRV}}(\omega) = H_{\hat{P}_{DRP}/P_{EP}}(\omega)H_{P_{EP}/E_{DRV}}(\omega) \tag{15}$$

6 Experimental Evaluation in Artificial Ears

We evaluated the proposed method in Type 2 GRAS 43AC ear simulator (one unit) and Type 4.3 Brüel & Kjaer Type 5128 head and torso simulator (HATS)

(two ears including pinna), as their designs are different [2]. We used a pair of JBL Live Beam 3 earphones, whose drivers and in-ear microphones were wired and connected to an Audio Precision APx525 audio analyzer. The source signal was a sine sweep over the whole audio frequency range. Both left and right earphones were calibrated in 4 tubes of diameter 7 mm and lengths 8, 15, 20, and 25 mm with several insertions. We estimated the matrix elements $[a_{11}(\omega), a_{12}(\omega)]$ of $\boldsymbol{T_{EP}}$ and $[d_{11}(\omega), d_{12}(\omega)]$ of $\boldsymbol{T_{EP2}}$ by using the calibration procedure described in Section 3, and averaging the results for the left and right earphones.

The following figures show the different steps of the method described in Sections 4 and 5. The pressure responses $H_{P_{MIC}/E_{DRV}}(\omega)$ of the in-ear microphones were measured for several insertions in the artificial ears, as illustrated in Fig. 2. The individual measurements are represented by light lines and the average by thick lines. These pressure responses were used to calculate the input ear impedances $Z_{EC}(\omega)$ and pressure responses $H_{P_{EP}/E_{DRV}}(\omega)$ at the ear tip, as illustrated in Figs. 3 and 4 respectively. After estimating the modal parameters from the inverse of the impedances $Z_{EC}(\omega)$, we designed the ear canal transfer functions $H_{\hat{P}_{DRP}/P_{EP}}(\omega)$ between the measured pressure at the ear tip and estimated pressure at DRP, as shown in Fig. 5. For the GRAS

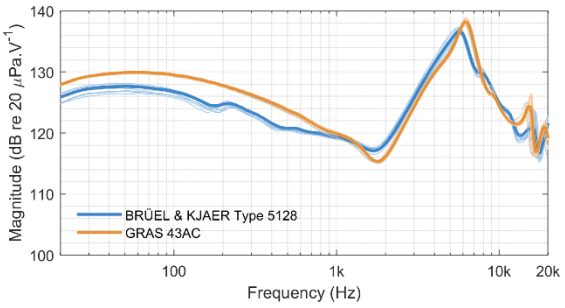


Figure 2. Measured pressure responses $H_{P_{MIC}/E_{DRV}}(\omega)$ of in-ear microphones in ear simulators.

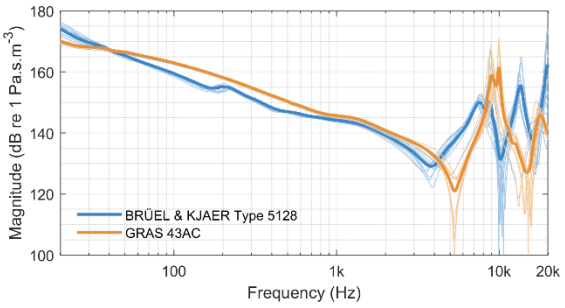


Figure 3. Measured ear impedances $Z_{EC}(\omega)$ at the ear tip in ear simulators.

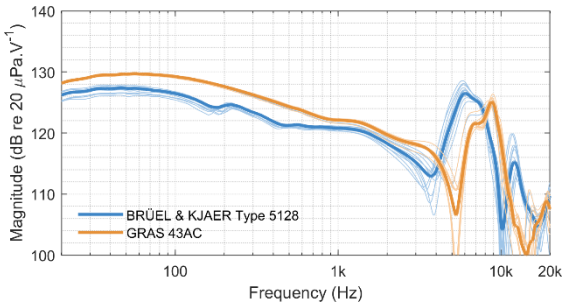


Figure 4. Measured pressure responses $H_{P_{EP}/E_{DRV}}(\omega)$ at the ear tip in ear simulators.

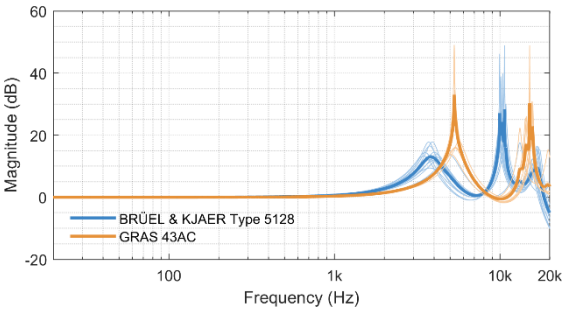


Figure 5. Estimated ear canal transfer functions $H_{\hat{P}_{DRP}/P_{EP}}(\omega)$ in ear simulators.

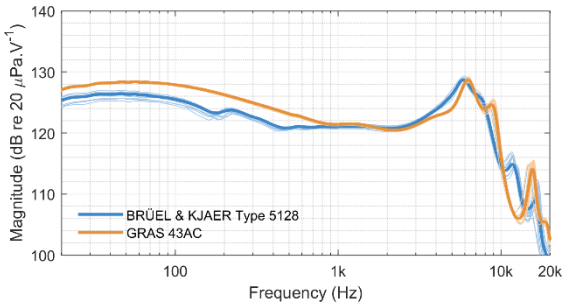


Figure 6. Measured pressure responses $H_{P_{DRP}/E_{DRV}}(\omega)$ at DRP in ear simulators.

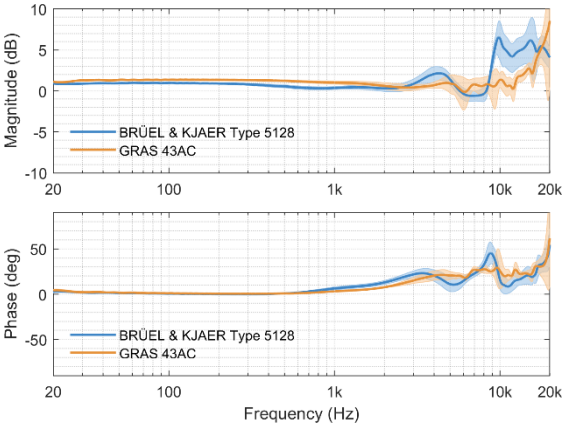


Figure 7. Error $\hat{P}_{DRP}(\omega)/P_{DRP}(\omega)$ in magnitude (top) and phase (bottom) in ear simulators (thick line: average, transparent area: standard deviation).

43AC ear simulator, we added a third eigenfrequency above 20 kHz to limit the pressure error. The measured pressure responses $H_{P_{DRP}/E_{DRV}}(\omega)$ at DRP are illustrated in Fig. 6. The error $\hat{P}_{DRP}(\omega)/P_{DRP}(\omega)$ in magnitude and phase are presented in Fig. 7, where the average is represented by thick lines and the standard deviation by transparent areas. We can see that the error is very low below the first ear canal resonance, then is+/- 3 dB and between 0° and 60° up to 9 kHz and increase in magnitude above this frequency. These levels of error may be caused by truncation of the modal expansion of Eq. (6) after 3 resonances.

We can take the opportunity to highlight the differences between the 2 types of artificial ears. The first resonance is higher in the GRAS 43AC ear simulator than in the Brüel & Kjaer Type 5128 HATS (5.3 kHz vs 3.8 kHz) as illustrated in Figs. 3 and 5, because of a shorter distance between the ear tip and the microphone at DRP. Also, the volume of the cavity in the Type 2 artificial ear is smaller resulting in a higher sound pressure level at low frequencies as highlighted in Figs. 2, 4, and 6.

Finally, the equivalent impedances at DRP, i.e. the 2 annular cavities in Type 2 and the 4 cavities around the microphone in Type 4.3 artificial ears, have different values as seen in the ear impedance between 800 Hz and 6 kHz in Fig. 3. As a result, they have a direct effect on the damping coefficient of the resonances as highlighted in the ear canal transfer functions in Fig. 5. Nevertheless, because of the coupling with the output impedance of the earphone [7], the differences are smaller for the pressure responses $H_{P_{DRP}/E_{DRV}}(\omega)$ at DRP in Fig. 7.

7 Experiments in Users' Ears

After evaluating the performance in artificial ears, we repeated the process for human ears. We measured the pressure responses $H_{P_{MIC}/E_{DRV}}(\omega)$ of in-ear microphones in 13 subjects, all adults, with several insertions of earphones in left and right ears. Then, we estimated the ear canal transfer functions and sound pressure at the eardrum, and we checked the consistency of the results between insertions for each ear. For ease of highlighting differences between sealed ears, we selected one insertion per ear and removed results with leakage at low frequencies, leaving 22 ears. We compared them with the estimated pressures in the artificial ears for one insertion in one ear as well. The results of measured ear impedance $Z_{EC}(\omega)$, estimated ear canal transfer function $H_{\hat{P}_{DRP}/P_{EP}}(\omega)$, and estimated pressure $H_{\hat{P}_{DRP}/E_{DRV}}(\omega)$ at the subjects' eardrums are illustrated in Figs. 8, 9, and 10 respectively.

We can see that the ear impedances and ear canal transfer functions in Figs. 8 and 9 vary significantly among the panel of subjects. The first closed ear canal resonances range from 2.2 kHz to 4.3 kHz and 8 to 17 dB, the second resonances range from 6.1 kHz to 11.4 kHz, and the third resonances from 11.0 kHz to 16.5 kHz. Ear canal transfer functions of one subject's ears dip to -8 dB between the first and second resonances, suggesting a "constricted" ear canal geometry (i.e. narrower diameter in the middle as seen in [5]). The range of estimated sound pressure levels (SPL) at DRP among subjects, seen in Fig. 10, is 7 dB at low frequencies, up to 11 dB between 1 kHz and 3 kHz, and can be up to 12 dB between 3 kHz and 9 kHz. We do not compare the high frequencies as the accuracy of estimated values decreases above 9 kHz.

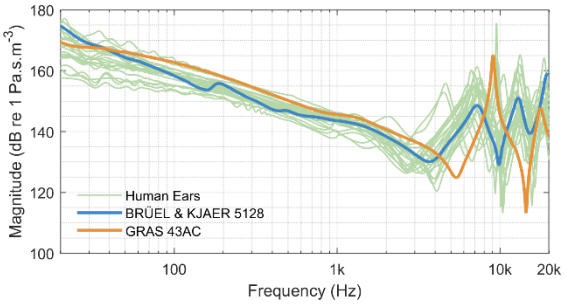


Figure 8. Measured input impedances $Z_{EC}(\omega)$ at the ear tip in subjects' ears and ear simulators.

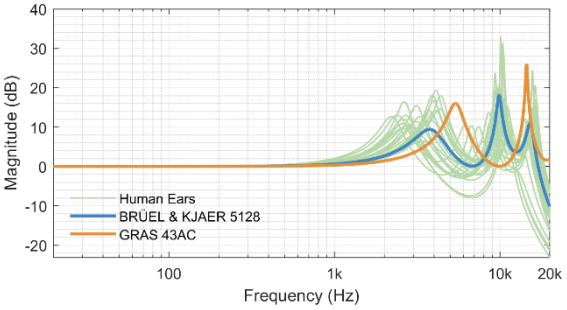


Figure 9. Estimated ear canal transfer functions $H_{\hat{P}_{DRP}/P_{EP}}(\omega)$ in subjects' ears and ear simulators.

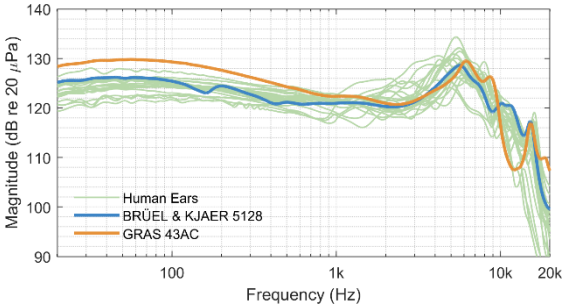


Figure 10. Estimated pressure responses $H_{\hat{P}_{DRP}/E_{DRV}}(\omega)$ at DRP in subjects' ears and ear simulators.

Finally, it is worth mentioning that while the Type 4.3 artificial ear does correspond to an average of human ears, the Type 2 artificial ear seems to be an outlier. It has only 2 closed ear canal resonances up to 20 kHz and the small ear canal volume results in a higher SPL than those in subjects' ears as seen in Fig. 10.

8 Discussion

We showed that we can get accurate results up to 9 kHz in Type 2 and Type 4.3 artificial ears. The main advantages of the proposed method are that the design of the earphone is not constrained, and that the ear canal transfer function, and therefore the pressure at DRP, can be found without making assumptions about canal geometry or eardrum impedance. Even though the use of the modal expansion cannot get the exact solution of the closed form due to the infinite sum [20], it has been shown that the approach is a good balance to get ear canal transfer function of different eardrum impedances and ear canal geometries with varying cross sections, while limiting the error in artificial ears. As the magnitude of the first resonance depends on the following ones, we observed that including 3 resonances was preferred to limit the error level at high frequencies. We only showed measurements with sealed ears, but the method allows us to estimate the sound pressure at the eardrum / DRP in presence of fit leakage at low frequencies.

We expressed the modal expansion of the pressure with the assumption that the eardrum is perpendicular to the x axis. Of course, anatomical ear geometry is more complex, with oblique incidence of waves near the eardrum. An internal investigation using finite element methods with COMSOL Multiphysics software that was based on [22] showed a decrease of the magnitude of the ear canal transfer function at high frequencies for a "true" physical eardrum model relative to our simplifying assumption of perpendicular eardrum incidence. These observations may explain the increase of errors above 10 kHz for the Type 4.3 artificial ear compared to the Type 2, suggesting that it is difficult to estimate the pressure at DRP above this frequency range as noted in [23].

The pressure response at DRP is potentially highly dependent on the electroacoustic elements of the earphone [7]. In contrast, the ear canal transfer function provided by this method is independent of the earphone. As a result, earphones with different output impedances may give different deviations of pressure at DRP as resonances are damped by the output impedance of the source.

Finally, we note that the standard deviation of estimated pressure at DRP in individual subjects' ears across insertions is less than 2 dB between 800 Hz and 6 kHz, and 6 dB between subjects. Variation across insertions could reflect the accuracy of the method, and likely also results from slightly different depths and angles between insertions that yield slightly different transfer functions. Regardless, the tight repeatability within ears, and the higher variation seen among ears, suggests that the method has capabilities to discern real differences.

9 Conclusion

We proposed a method to estimate both the ear canal transfer function and sound pressure at the eardrum using earphones. A calibration process was introduced to turn the earphones into pressure-volume velocity sensors. The measured input ear impedance allows estimation of the eigenfrequencies and modal parameters, in turn useful in a simple expression of the ear canal transfer function as the sum over the first modes. Measurements in artificial ears showed promising results while maintaining reasonable sound pressure level errors at the drum reference point up to 9 kHz. These preliminary results pave the way for applications of personalized compensation functions for the users and even hearing pathology screenings.

Acknowledgements

The authors would like to thank the Harman Research group who supported this research work and all the colleagues, especially Christian Garcia, who made significant contributions.

References

[1] S. Olive, "A comparison of in-ear headphone target curves for the Brüel & Kjær Head & Torso Simulator Type 5128," in *Audio Engineering Society 157th Convention*, 2024.

[2] "ITU-T Rec. P. 57 - P series: Telephone transmission quality, telephone installations, local line networks - Artificial ears," 06/2021.

[3] S. Jønsson, A. Schuhmacher and H. I. Jørgensen, "Wideband impedance measurement in the human ear canal; In vivo study on 32 subjects.," *arXiv preprint arXiv:1811.03389,* 2018.

[4] M. Stinson and B. Lawton, "Specification of the geometry of the human ear canal for the prediction of sound-pressure level distribution," *The Journal of the Acoustical Society of America, 85(6),* pp. 2492-2503, 1989.

[5] S. Voss, A. Remenschneider, R. Farrar, S. Myoung and N. Horton, "Comprehensive Measurements and Analyses of Ear Canal Geometry From Late Infancy Through Late Adulthood: Age-Related Variations and Implications for Basic Science and Audiological Measurements," *Trends in Hearing, 29,* 2025.

[6] S. Voss, J. Rosowski, S. Merchant and W. Peake, "Acoustic responses of the human middle ear," *Hearing research,* vol. 150, no. 1-2, pp. 43-69, 2000.

[7] T. Zurbrugg, A. Holzl, S. Kohler and S. Harsch, "Acoustic output impedance as a measure for independency of individual acoustic ear conditions.," in *Forum Acusticum (pp. 2907-2912),* 2020.

[8] J. Chan and C. Geisler, "Estimation of eardrum acoustic pressure and of ear canal length from remote points in the canal," *The Journal of the Acoustical Society of America, 87(3),* pp. 1237-1247, 1990.

[9] T. Sankowsky-Rothe, M. Blau, E. Rasumow, H. Mojallal, M. Teschner and C. Thiele, "Prediction of the sound pressure at the ear drum in occluded human ears.," *Acta acustica united with Acustica 97.4,* pp. 656-668, 2011.

[10] H. Horbach and K. Amini Khoiy, "Auto-calibrating in-ear headphone". Patent US11736861B2, 2021.

[11] H. Hudde, A. Engel and A. Lodwig, "Methods for estimating the sound pressure at the eardrum," *The Journal of the Acoustical Society of America,* vol. 106, no. 4, pp. 1977--1992, 1999.

[12] N. Wulbusch, R. Roden, A. Chernov and M. Blau, "Using a one-dimensional finite-element approximation of Webster's horn equation to estimate individual ear canal acoustic transfer from input impedances.," *The Journal of the Acoustical Society of America, 153(5),* pp. 2826-2826, 2023.

[13] K. Nørgaard, K. Charaziak and C. Shera, "A comparison of ear-canal-reflectance measurement methods in an ear simulator," *The Journal of the Acoustical Society of America,* vol. 146, no. 2, pp. 1350-1361, 2019.

[14] S. Vogl and M. Blau, "Individualized prediction of the sound pressure at the eardrum for an earpiece with integrated receivers and microphones.," *The Journal of the Acoustical Society of America, 145(2),* pp. 917-930, 2019.

[15] N. N. Souza, S. Dhar, S. T. Neely and J. H. Siegel, "Comparison of nine methods to estimate ear-canal stimulus levels.," *The Journal of the Acoustical Society of America, 136(4),* pp. 1768-1787, 2014.

[16] J. G. Bolaños and V. Pulkki, "Estimation of pressure at the eardrum in magnitude and phase for headphone equalization using pressure-velocity measurements at the ear canal entrance," in *2015 IEEE Workshop on Applications of Signal Processing to Audio and Acoustics (WASPAA).*, 2015.

[17] A. Bezzola, "In-Ear Headphones on Ear Canal Simulator vs Real Human Ear Geometries: Quantifying the Differences with Simulations," in *Audio Engineering Society Convention 155*, 2023.

[18] I. Wils, A. Geerardyn, T. Putzeys, K. Denis and N. Verhaert, "Lumped element models of sound conduction in the human ear: A systematic review," *The Journal of the Acoustical Society of America, 154(3),* pp. 1696-1709, 2023.

[19] Y. Xia, Z. Guo, E. Tiana-Roig, V. Henriquez and F. Lucklum, "Effect of curvature on sound propagation in the ear canal," *The Journal of the Acoustical Society of America, 155(1),* pp. 695-706, 2024.

[20] A. Chaigne and J. Kergomard, Acoustics of musical instruments, Springer, 2016.

[21] M. H. Richardson and D. L. Formenti, "Parameter estimation from frequency response measurements using rational fraction polynomials.," in *Proceedings of the 1st international modal analysis conference (Vol. 1, pp. 167-186),* Union College Schenectady, NY, 1982.

[22] L. B. Nielsen and M. H. Jensen, "The Digital Twin of a New and Standardized Fullband Ear Simulator," in *DAGA*, Stuttgart, 2022.

[23] K. Nørgaard, H. Motallebzadeh and S. Puria, "The influence of tympanic-membrane orientation on acoustic ear-canal quantities: A finite-element analysis," *The Journal of the Acoustical Society of America, 155(4),* pp. 2769-2785, 2024.